Fibroblast Activation Protein Imaging in Reperfused ST-Elevation Myocardial Infarction: Comparison with Cardiac Magnetic Resonance Imaging

Boqia Xie
Beijing Chao-Yang Hospital Capital Medical University: Beijing Chaoyang Hospital
Jiaxin Wang
Fuwai Hospital State Key Laboratory of Cardiovascular Disease
Xiao-Ying Xi
Beijing Chao-Yang Hospital Capital Medical University: Beijing Chaoyang Hospital
Xiaojuan Guo
Beijing Chao-Yang Hospital Capital Medical University: Beijing Chaoyang Hospital
Bi-Xi Chen
Beijing Chao-Yang Hospital Capital Medical University: Beijing Chaoyang Hospital
Cuncun Hua
Beijing Chao-Yang Hospital Capital Medical University: Beijing Chaoyang Hospital
Shihua Zhao
Fuwai Hospital State Key Laboratory of Cardiovascular Disease
Pixiong Su
Beijing Chao-Yang Hospital Capital Medical University: Beijing Chaoyang Hospital
Mulei Chen
Beijing Chao-Yang Hospital Capital Medical University: Beijing Chaoyang Hospital
Min-Fu Yang (minfuyang@126.com)
Beijing Chaoyang Hospital https://orcid.org/0000-0002-9015-0541

Research Article

Keywords: Fibroblast activation protein inhibitor, Fibroblast, Cardiovascular magnetic resonance, ST-elevation myocardial infarction, Cardiac functional recovery

Posted Date: October 14th, 2021

DOI: https://doi.org/10.21203/rs.3.rs-964242/v1

Version of Record: A version of this preprint was published at European Journal of Nuclear Medicine and Molecular Imaging on January 5th, 2022. See the published version at https://doi.org/10.1007/s00259-021-05674-9.

Abstract

Purpose

The goals were to explore the correlation of ^{18}F-labeled fibroblast activation protein inhibitor (FAPI) and cardiovascular magnetic resonance (CMR) parameters in ST-elevation myocardial infarction (STEMI) patients with successful primary percutaneous coronary intervention (PPCI) and to investigate the value of FAPI imaging in predicting cardiac functional recovery.

Methods

Fourteen first-time STEMI patients (11 men, mean age: 62 ± 11 years) after PPCI were prospectively recruited. All patients underwent baseline FAPI imaging (6 ± 2 days post-MI) and CMR (8 ± 2 days post-MI). Ten patients had convalescent CMR (84 ± 4 days post-MI). Myocardial FAPI activity was analyzed on extent (the percentage of FAPI uptake volume over the left ventricular volume, FAPI%), intensity (target-to-background uptake ratio, TBRmax), and amount (FAPI%×TBRmax). Serum biomarkers during the acute phase, late gadolinium enhancement (LGE), T2-weighted imaging (T2WI), extracellular volume (ECV), microvascular obstruction (MVO), and cardiac function from CMR imaging were analyzed.

Results

Localized but inhomogeneous FAPI uptake was observed, which was larger than the edematous and infarcted myocardium. The MVO area showed lower FAPI uptake compared with the surrounding myocardium. FAPI activity was associated with myocardial injury biomarkers, T2WI, LGE, and ECV at both per-patient and per-segment levels (all $p < 0.05$). Among the CMR parameters, T2WI had the greatest correlation coefficient with both FAPI% and FAPI%×TBRmax. Baseline TBRmax was correlated with convalescent left ventricular ejection fraction (LVEF)($r = -0.73$, $p = 0.02$).

Conclusion

FAPI imaging detects more involved myocardium than CMR in reperfused STEMI, and was associated with myocardial damage and convalescent LVEF.

Introduction

ST-elevation myocardial infarction (STEMI) triggers an orchestrated and complicated series of events from the initial sterile inflammation to the subsequent (myo)fibroblast proliferation and scar formation [1]. Appropriate fibrotic response following MI preserves the structural integrity, whilst excessive or prolonged fibrogenic activation leads to adverse ventricular remodeling.

Cardiac magnetic resonance (CMR) is a reliable technique for the evaluation of pathological changes of post-MI myocardium using different sequences and modalities: late gadolinium enhancement (LGE) for scar and focal fibrosis [2, 3], T2-weighted imaging (T2WI) and T2 mapping for edema, and extracellular volume (ECV) derived from T1-weighted imaging for the total interstitial space [2]. However, these imaging sequences reflects the increase of extracellular matrix components but not the central cellular effectors of fibrosis–the fibroblasts.

Fibroblasts undergo dramatic phenotypic changes following MI, in addition to its traditional role as the main source of extracellular matrix proteins, recent evidence has suggested that activated fibroblasts may regulate inflammation, modulate cardiomyocyte survival, and mediate angiogenesis [4-6]. These features made fibroblast the crucial cell in both repair and pathogenesis of adverse remodeling. Fibroblast activation protein (FAP) is a membrane-anchored peptidase that is specifically expressed by activated fibroblasts [7], and lately, radiolabelled FAP inhibitor (FAPI)-targeting tracer have been developed to detect the activated fibroblasts [8]. These tracers have been widely used for positron emission tomography/computed tomography (PET/CT) imaging in various diseases especially cancer, and recently in cardiac diseases [9, 10]. Several pre-clinical and clinical studies reported that MI would induce enhanced FAPI uptake, which extended over the culprit territory and the LGE area [11-14], these findings suggested FAPI imaging may have unique advantage in detecting the affected myocardium.

Nevertheless, some concerns of FAPI imaging in MI remained. First, previous comparison with CMR was limited to LGE, since new sequences have been proved more accurate in evaluating myocardial injury, their comparisons with FAPI should be clarified. Second, the prognostic value of FAPI imaging in post-MI cardiac recovery needs to be explored.

Therefore, we tried to explore the correlation of FAPI imaging and CMR parameters in reperfused STEMI patients, within two weeks of the MI event. We then investigated the prognostic value of FAPI imaging in cardiac recovery at 3-month post-MI.

Materials And Methods

Study population

This prospective study was approved by the Institutional Ethical Committee of Beijing Chaoyang Hospital (2020-ke-225) and was performed in agreement with the Declaration of Helsinki. From January to February 2021, we recruited 14 consecutive first-time STEMI patients (11 men, mean age: 62 ± 11 years) successfully treated by primary percutaneous coronary intervention (PPCI) < 12 hours from the onset of symptoms at Beijing Chaoyang Hospital. Diagnosis and treatment of STEMI were as per current guidelines [15, 16]. Exclusion criteria were < 18 years of age, previous cardiac events (myocardial infarction,

cardiac surgery, PCI), valvular diseases, cardiomyopathies, abnormal renal function, or contraindications to the use of gadolinium-based contrast agents or CMR. All patients underwent baseline myocardial ^{18}F-AIF-NOTA-FAPI PET/CT imaging (6 ± 2 days post MI) and CMR (8 ± 2 days post MI). Ten patients had convalescent CMR scans (84 ± 4 days post MI). Patients or their guardians signed the informed consent before enrollment in the study.

Blood analysis

Serial blood samples were tested in all patients at admission and in the cardiac care unit before transferring the patients to ordinary wards, including complete blood count, metabolic panel (troponin I, creatine kinase-MB [CK-MB], creatine kinase [CK], B-type natriuretic peptide [BNP], lactate dehydrogenase [LDH], cholesterol and triglyceride levels, liver and renal function tests), and arterial blood gas tests.

FAPI images acquisition and interpretation

^{18}F-AIF-NOTA-FAPI was radio-labelled as previously described [17]. PET/CT images were acquired 60 minutes after injection (2.5-3.0 MBq/kg) using a 16-slice PET/CT scanner (Discovery STE, GE, USA). CT parameters were 140 kV, 120 mA, pitch 1.375, 16 ×0.625 mm collimation, and section width of 5 mm. Two beds of PET images (5 min/bed, 3D mode) were acquired, and the heart was set in the center of the view. Attenuation-corrected PET images (voxel size, 3.9 × 3.9 × 3.3 mm) were reconstructed from the CT data using a 3D ordered-subset expectation maximization algorithm (14 subsets, 2 iterations). Integrated PET and CT images were obtained automatically on AW VolumeShare 2 (GE Healthcare).

FAPI images were independently evaluated by two nuclear physicians (XYX and MFY) blinded to the CMR and clinical information. Disagreements were resolved by consensus. Myocardial FAPI uptake was analyzed in the global and segmental manner, respectively. For global analysis, a volume of interest (VOI) was manually drawn around the myocardium with FAPI uptake, and a region grow algorithm with a threshold of 50% of the maximum uptake was set to determine the FAPI volume. The FAPI volume was further expressed as a percentage of left ventricular (LV) volume derived from MRI–this percentage was defined as the FAPI extent (FAPI%). Within this VOI, the maximum standardized uptake values (SUVmax) were automatically derived, and a target-to-background ratio (TBRmax) was calculated by dividing myocardial SUVmax by blood pool SUVmean to indicate the FAPI intensity. Finally, the total FAPI was calculated by the product of FAPI% and FAPI TBRmax.

For segmental analysis, the American Heart Association 17-segment model was applied using QPS software (version 3.1, Cedars-Sinai Medical Center, Los Angeles, CA, USA). Segmental FAPI uptake was automatically calculated by the software and expressed as a percentage of the LV SUVmax, and the product of this percentage and LV TBRmax was further calculated to represent the segmental TBRmax.

CMR image acquisition and interpretation

CMR was performed on a 3.0-T scanner (Prisma, Erlangen, Siemens Healthcare, Germany) using the following protocol: balanced steady-state free precession (bSSFP) acquisitions for long- and short-axis cine; short time inversion recovery (STIR) prepared T2WI of three short axis slices (basal, mid-ventricular and apical); standard LGE imaging matching long- and short-axis bSSFP cine slices for the quantification of scar burden; and modified Look-Locker inversion recovery (MOLLI) sequence for pre- and post-contrast T1 mapping of 3 short-axis slices. LGE and post-contrast T1 mapping images were collected 10-15 min after the administration of 0.1 mmol/kg Gd-DOTA (Dotarem^{TM}, Guerbet S.A., Paris, France). Typical acquisition parameters for bSSFP were TE/TR = 1.4/44 ms, flip angle 44°, voxel size 0.8 × 0.8 × 8.0 mm, and matrix 192 × 256. Parameters for STIR-prepared T2WI were TE/TR = 50/2100 ms, voxel size 1.4 × 1.4 × 8.0 mm, and matrix 135 × 256. The MOLLI acquisition followed the 5(3)3 protocol for pre-contrast and the 4(1)3(1)2 protocol for post-contrast T1 mapping with typical parameters of TE/TR = 1.12/283 ms, voxel size 1.4 × 1.4 × 8.0 mm, and matrix 148 × 256. The LGE parameters were TE/TR = 1.96/450 ms, flip angle 20°, and voxel size 1.4 × 1.4 × 8.0 mm.

CMR images were analyzed on a commercial software (Cvi42, Version 5.12.2, Circle Cardiovascular Imaging Inc., Calgary, Canada) by two experienced CMR operators (JXW and SHZ) who were blinded to both clinical and FAPI data; disagreements were resolved by consensus. Volumetric and functional parameters were calculated from the cine images. The infarcted myocardium was identified on LGE images using 5 SD above the remote myocardium [14]. Myocardial edema was defined by a high signal intensity on T2WI two standard deviations (SD) above the signal intensity of the remote myocardium. The extent of T2WI and LGE was expressed as the percentage of LV mass (T2WI% and LGE%). Microvascular obstruction (MVO) was identified in LGE images as hypointense recesses within the hyperenhanced myocardium. ECV were quantified according to the established formula [18]: ECV = (1 – hematocrit) × ($1/T1_{myopost}$ – $1/T1_{myopre}$) / ($1/T1_{bloodpost}$ – $1/T1_{bloodnative}$) and expressed as ECV%. The apex segment was excluded in the segment-to-segment comparative analysis between FAPI and CMR images.

Statistical analysis

SPSS Statistics (Version 24; IBM) was adopted. The normality of distribution was assessed by Kolmogorov–Smirnov test. Continuous variables were described as mean (SD) or medians (ranges), depending on the normality of distribution. Categorical variables were expressed as absolute numbers and percentages. A paired *t* test was used to compare the different imaging parameters in the same individual. ANOVA and non-parametric tests were used to compare the differences of parameters among segments. Pearson/Spearman's correlation analysis was conducted to explore the relationship. Boxplot was used to determine the outliers. A p-value < 0.05 was considered to be statistically significant.

Results

Patients' characteristics

Detailed characteristics of the 14 patients are presented in **Table 1**. Culprit lesion was determined at the left main coronary artery in 1 patient (7.10%), left anterior descending coronary artery in 10 patients (71.40%), and right coronary artery in 3 patients (21.40%). The pain-to-balloon time was 6 hours (3-11 hours). Four patients' peak troponin levels exceeded the measurable upper limit and were reported as >500 ng/mL. The remaining 10 patients' peak troponin level was 158 ± 40 ng/mL. All patients were taking aspirin, clopidogrel/ticagrelor, and statin at discharge.

Strong correlation was demonstrated between FAPI% and CKMBmax, maximum white blood cell count (WBCmax), LDHmax (r values of 0.79, 0.65, and 0.62; all $p < 0.05$), followed by a moderate correlation between FAPI%×TBRmax and CKMBmax, WBCmax, LDHmax and BNPmax (r values of 0.56, 0.55, 0.56 and 0.59; all $p < 0.05$) (**Table 2**). TBRmax was found only related to WBCmax ($r = 0.59$, $p = 0.03$).

Comparison of FAPI and CMR

Localized but inhomogeneous FAPI uptake was observed in all patients (**Fig. 1**). The FAPI% varied to a larger scale (20.82%-78.74%) even in patients with similar culprit lesion. Notably, the FAPI% was larger than T2WI% (45.03% ± 16.23% versus 24.80% ± 6.73%, $p < 0.001$) and LGE% (19.79% ± 8.26%, $p = 0.03$) (**Fig. 2B**). When FAPI% increased, the differences between FAPI% and T2WI%, LGE%, ECV% raised (all $p < 0.001$) (**Fig. 2C**).

On patient level, FAPI% had stronger correlation with CMR parameters than FAPI%×TBRmax and TBRmax (**Table 3**). Among the CMR parameters, T2WI% had the greatest correlation coefficient with both FAPI% and FAPI%×TBRmax (r values of 0.83 and 0.83; both $p < 0.05$).

On segment level (**Fig. 3**), significant correlations were demonstrated between segmental TBRmax and T2WI%, LGE%, ECV% (r values of 0.62, 0.79 and 0.71; all $p < 0.001$). MVO were observed in 21 segments in four patients. FAPI uptake in the MVO area was lower than in the surrounding tissue (**Fig. 4**).

Follow-up

Improvement was recorded in LVEF (47.84% ± 12.10% versus 55.39% ± 7.93%, $p = 0.01$). After exclusion of one outlier in the follow-up LVEF in patient No.11. Baseline TBRmax, ECV% and T2WI% were found related to the convalescent LVEF (r values of -0.73, -0.74, and -0.70; all $p < 0.05$) (**Table 4** and **Fig. 5**).

Discussion

Noninvasive imaging plays an essential role in the monitoring of post-MI myocardial remodeling. Using gallium-68 (^{68}Ga)-labeled FAPI, Varasteh and coworkers demonstrated excellent in vivo imaging quality for the detection of post-MI fibroblast activation in a MI rat model [11]. More recently, the feasibility of ^{68}Ga-FAPI imaging in MI patients was reported by Notohamiprodjo [12], Kessler [13], and Diekmann [14], which identified intense FAPI uptake in the infarcted territory. These data suggest that FAPI imaging is a reliable technique in delineating the temporospatial status of activated fibroblasts and may help to better explain post-MI pathophysiologic evolution and monitoring of the efficacy of antifibrotic therapies.

Reperfused MI induced an extending FAPI uptake over the infarct region

Previous reports [12, 14] demonstrated an extended fibroblasts activation over the perfusion defect and LGE area. In the current study, by comparing with multiple CMR sequences, we further identified that the FAPI uptake extent was even larger than the edematous area. Our finding was in line with Kessler's study [13], who reported FAPI uptake in the non-culprit territory.

Fibroblasts are sensitive to local chemical and mechanical stimulations. Acute MI induces an intense inflammatory reaction in the infarcted region and upregulates the levels of TGF-β1, IL-1β, and IFNγ in the jeopardize area along with increased mechanical load [19, 20] contributing to fibroblast activation. Although the abundant cardiac resident fibroblasts located closely to the vessels are important cellular effectors responded to the activating signals following MI. Recent data from animal experiments suggested the intense upregulation of chemokines induced by MI may drive recruitment of non-resident fibroblasts that may significantly contribute to the expansion of activated fibroblasts. As been reported by Nagaraju and coworkers in a MI pig model [21], upregulated expression of TGF-β1–a strong stimulator for fibroblast differentiation–and positive FAP-α staining were seen in the border and remote myocardium in addition to the scar region, suggesting the activation of fibroblasts could occur in the non-infarcted area. Future studies are needed to explore the signal pathways mediating fibroblasts activation in the non-culprit territory, and to illustrate their functions.

FAPI uptake was associated with the degree of myocardial injury

Our data showed that both the extent and amount of FAPI uptake were strongly correlated with myocardial injury assessed by serum biomarkers and CMR-derived parameters, and systemic inflammation. As been discussed above, upregulated chemokines and increased mechanical stress induced by MI are strong stimulators of fibroblasts, and inflammatory cells as macrophages and mast cells also play an important role in fibroblast activation by secreting various bioactive mediators [22]. These facts explained the tight association between myocardial damage and FAPI uptake, and FAPI imaging a reliable modality in evaluating reperfused myocardial damage. Although our findings concerning the correlation of FAPI uptake and serum biomarkers were in line with Kessler's results [13], they were different from Diekmann's report [14]. A more detailed data presentation from the latter may help in better interpretation of the differences.

FAPI and convalescent cardiac function

To our best knowledge, we reported for the first time that FAPI imaging has prognostic value in post-MI cardiac recovery. The correlation coefficient of FAPI uptake intensity was not inferior to the well-established CMR predictors. However, our data cannot explain why baseline FAPI uptake extent was not associated with convalescent LVEF even though its relationship was stronger than FAPI uptake intensity with the CMR predictors. The traditional concept of cardiac fibroblast as the manufactory of extracellular matrix proteins has been challenged by growing evidence suggesting that fibroblasts are functionally and

phenotypically heterogeneous, which exerts diverse effects in the complex post-MI signal pathways [2-4]. Therefore, we presume the fibroblasts in the infarct, border, and remote myocardium maybe functional and phenotypical distinct, thus leading to inconsistent or even contrary effects on post-MI prognosis, which may partially explain why the extent of FAPI uptake was not predictive of cardiac recovery.

Although animal experiments showed that myocardial FAPI uptake declined significantly at six days post-MI [11], human-based clinical studies [13] show that FAPI activity can be detected on the 66th day post-infarction. Continued activation of fibroblasts may play an essential role in the cardiac remodeling. Unfortunately, repeated FAPI imaging was not performed in the convalescent phase in our patients. The evolution of FAPI uptake in STEMI patients with PPCI in the real world needs further exploration. Future studies aimed at the temporal alterations of post-MI FAPI imaging and its correlation to the cardiac remodeling will provide useful theoretical evidence and improve our knowledge of post-MI remodeling.

MVO could be visualized by FAPI imaging

Ischemia-reperfusion injurie could result in coronary microvascular obstruction, leading to a significant reduction or occlusion of effective blood flow to the affected regions [23]. Accordingly, we assume the delivery of FAPI tracer to the MVO area also declined and resulted in the hypo-uptake region within the culprit territory.

MVO is an important predictor of cardiac mortality and the therapeutic target in STEMI patients undergoing PPCI. First-pass perfusion and LGE by CMR were two techniques used to detect MVO [24]. However, first-pass perfusion is limited by the low spatial resolution and signal-to-noise ratio, and LGE is limited in terms of longer examination time and multiple breath holds. This study, to our knowledge, proposed for the first time that MVO could be visualized by FAPI imaging. However, restricted to the limited number, the feasibility of FAPI imaging in detecting MVO needs further validation.

Limitations

This study has several limitations. First, the sample size was small: only 14 patients were included in the FAPI-CMR comparison, and only 10 patients had repeated CMR scans. Second, FAPI and CMR were not simultaneously performed, which may affect the comparability of the results. Third, FAPI imaging was not repeated in the follow-up period. A multicentered cohort study enrolling more STEMI patients with an extended follow-up period may yield more information on post-MI FAPI imaging.

Conclusions

In reperfused STEMI patients, by comparing FAPI imaging and CMR, we demonstrated that activated fibroblasts existed in the non-edematous or infarcted myocardium. As a new modality, FAPI imaging is feasible in assessing myocardial damage and has prognostic value in post-MI cardiac recovery, these advantages made it a potential technique in the evaluation of myocardial remodeling after MI and a favorable method in analyzing fibroblast-targeted antifibrotic therapies.

Declarations

Conflicts of interest The authors do not have any conflicts of interest to declare.

Ethics approval All procedures involving human participants were carried out in accordance with the ethical standards of the institutional and/or national research committee and with the 1964 Helsinki Declaration and its later amendments or comparable ethical standards.

Consent to participate Informed consent was obtained from all individual participants included in the study.

Consent for publication Patients signed informed consent regarding publishing their data and photographs.

Availability of data and material The data underlying this article will be shared on reasonable request to the corresponding author.

Code availability Not applicable.

Authors' contribution Boqia Xie, Jiaxin Wang, Xiao-Ying Xi, Mulei Chen, and Min-Fu Yang wrote the draft of the manuscript; Boqia Xie, Jiaxin Wang, Xiao-Ying Xi, Xiaojuan Guo, Bi-Xi Chen, Cuncun Hua, and Pixiong SU collected and analyzed the clinical data; Jiaxin Wang, Xiaojuan Guo, and Shihua Zhao analyzed the CMR data, Xiao-Ying Xi, Bi-Xi Chen, and Min-Fu Yang analyzed the PET/CT data; Boqia Xie, Pixiong Su, Mulei Chen, and Min-Fu Yang conceived the study and interpreted the results. All authors contributed to the article's revision, agreed to its submission, and had full access to original data.

Funding: This work was supported by Beijing Hospitals Authority Clinical Medicine Development of Special Funding Support (ZYLX202105).

References

1. Prabhu SD, Frangogiannis NG. The biological basis for cardiac repair after myocardial infarction: from inflammation to fibrosis. Circ Res. 2016;119:91-112. https://doi.org/10.1161/CIRCRESAHA.116.303577.
2. Kali A, Cokic I, Tang RL, Yang HJ, Sharif B, Marbán E, et al. Determination of location, size, and transmurality of chronic myocardial infarction without exogenous contrast media by using cardiac magnetic resonance imaging at 3T. Circ Cardiovasc Imaging. 2014;7:471-481. https://doi.org/10.1161/CIRCIMAGING.113.001541.

3. Gupta S, Ge Y, Singh A, Gräni C, Kwong RY. Multimodality imaging assessment of myocardial fibrosis. JACC Cardiovasc Imaging. 2021. https://doi.org/10.1016/j.jcmg.2021.01.027.
4. Shinde AV, Frangogiannis NG. Mechanisms of fibroblast activation in the remodeling myocardium. Curr Pathobiol Rep. 2017;5:145-152. https://doi.org/10.1007/s40139-017-0132-z.
5. Nakaya M, Watari K, Tajima M, Nakaya T, Matsuda S, Ohara H, et al. Cardiac myofibroblast engulfment of dead cells facilitates recovery after myocardial infarction. J Clin Invest. 2017;127:383–401. https://doi.org/10.1172/JCI83822.
6. Ubil E, Duan J, Pillai IC, Rosa-Garrido M, Wu Y, Bargiacchi F, et al. Mesenchymal-endothelial transition contributes to cardiac neovascularization. Nature. 2014;514:585–590. https://doi.org/10.1038/nature13839.
7. Toms J, Kogler J, Maschauer S, Daniel C, Schmidkonz C, Kuwert T, et al. Targeting fibroblast activation protein: radiosynthesis and preclinical evaluation of an ^{18}F-labeled FAP inhibitor. J Nucl Med. 2020;61:1806-1813. https://doi.org/10.2967/jnumed.120.242958.
8. Altmann A, Haberkorn U, Siveke J. The latest developments in imaging of fibroblast activation protein. J Nucl Med. 2021;62:160-167. https://doi.org/10.2967/jnumed.120.244806.
9. Tillmanns J, Hoffmann D, Habbaba Y, Schmitto JD, Sedding D, Fraccarollo D, et al. Fibroblast activation protein alpha expression identifies activated fibroblasts after myocardial infarction. J Mol Cell Cardiol. 2015;87:194-203. https://doi.org/10.1016/j.yjmcc.2015.08.016.
10. Tallquist MD, Molkentin JD. Redefining the identity of cardiac fibroblasts. Nat Rev Cardiol. 2017;14:484-491. https://doi.org/10.1038/nrcardio.2017.57.
11. Varasteh Z, Mohanta S, Robu S, Braeuer M, Li Y, Omidvari N, et al. Molecular imaging of fibroblast activity after myocardial infarction using a ^{68}Ga-labeled fibroblast activation protein inhibitor, FAPI-04. J Nucl Med. 2019;60:1743-1749. https://doi.org/10.2967/jnumed.119.226993.
12. Notohamiprodjo S, Nekolla SG, Robu S, Villagran Asiares A, Kupatt C, Ibrahim T, et al. Imaging of cardiac fibroblast activation in a patient after acute myocardial infarction using ^{68}Ga-FAPI-04. J Nucl Cardiol. 2021. https://doi.org/10.1007/s12350-021-02603-z.
13. Kessler L, Kupusovic J, Ferdinandus J, Hirmas N, Umutlu L, Zarrad F, et al. Visualization of fibroblast activation after myocardial infarction using 68Ga-FAPI PET. Clin Nucl Med. 2021;46:807-813. https://doi.org/10.1097/RLU.0000000000003745.
14. Diekmann J, Koenig T, Zwadlo C, Derlin T, Neuser J, Thackeray JT, et al. Molecular imaging identifies fibroblast activation beyond the infarct region after acute myocardial infarction. J Am Coll Cardiol. 2021;77:1835-1837. https://doi.org/10.1016/j.jacc.2021.02.019.
15. Levine GN, Bates ER, Blankenship JC, Bailey SR, Bittl JA, Cercek B, et al. 2015 ACC/AHA/SCAI focused update on primary percutaneous coronary intervention for patients with ST-elevation myocardial infarction: an update of the 2011 ACCF/AHA/SCAI guideline for percutaneous coronary intervention and the 2013 ACCF/AHA guideline for the management of ST-elevation myocardial infarction: a report of the American College of Cardiology/American Heart Association Task Force on Clinical Practice Guidelines and the Society for Cardiovascular Angiography and Interventions. Catheter Cardiovasc Interv. 2016;87:1001-1019. https://doi.org/10.1002/ccd.26325.
16. Ibanez B, James S, Agewall S, Antunes MJ, Bucciarelli-Ducci C, Bueno H, et al. 2017 ESC guidelines for the management of acute myocardial infarction in patients presenting with ST-segment elevation: the task force for the management of acute myocardial infarction in patients presenting with ST-segment elevation of the European Society of Cardiology (ESC). Eur Heart J. 2018;39:119-177. https://doi.org/10.1093/eurheartj/ehx393.
17. Wang S, Zhou X, Xu X, Ding J, Liu S, Hou X, et al. Clinical translational evaluation of Al^{18}F-NOTA-FAPI for fibroblast activation protein-targeted tumour imaging. Eur J Nucl Med Mol Imaging. 2021. https://doi.org/10.1007/s00259-021-05470-5.
18. Flett AS, Hayward MP, Ashworth MT, Hansen MS, Taylor AM, Elliott PM, et al. Equilibrium contrast cardiovascular magnetic resonance for the measurement of diffuse myocardial fibrosis: preliminary validation in humans. Circulation. 2010;122:138-44. https://doi.org/10.1161/CIRCULATIONAHA.109.930636.
19. Kawaguchi M, Takahashi M, Hata T, Kashima Y, Usui F, Morimoto H, et al. Inflammasome activation of cardiac fibroblasts is essential for myocardial ischemia/reperfusion injury. Circulation. 2011;123:594-604. https://doi.org/10.1161/CIRCULATIONAHA.110.982777.
20. Siwik DA, Chang DL, Colucci WS. Interleukin-1beta and tumor necrosis factor-alpha decrease collagen synthesis and increase matrix metalloproteinase activity in cardiac fibroblasts in vitro. Circ Res. 2000;86:1259-1265. https://doi.org/10.1161/01.res.86.12.1259.
21. Nagaraju CK, Dries E, Popovic N, Singh AA, Haemers P, Roderick HL, et al. Global fibroblast activation throughout the left ventricle but localized fibrosis after myocardial infarction. Sci Rep. 2017;7:10801. https://doi.org/10.1038/s41598-017-09790-1.
22. Saxena A, Chen W, Su Y, Rai V, Uche OU, Li N, et al. IL-1 induces proinflammatory leukocyte infiltration and regulates fibroblast phenotype in the infarcted myocardium. J Immunol. 2013;191:4838–4848. https://doi.org/10.4049/jimmunol.1300725.
23. Judd RM, Lugo-Olivieri CH, Arai M, Kondo T, Croisille P, Lima JA, et al. Physiological basis of myocardial contrast enhancement in fast magnetic resonance images of 2-day-old reperfused canine infarcts. Circulation. 1995;92:1902-1910. https://doi.org/10.1161/01.cir.92.7.1902.
24. Nijveldt R, Hofman MB, Hirsch A, Beek AM, Umans VA, Algra PR, et al. Assessment of microvascular obstruction and prediction of short-term remodeling after acute myocardial infarction: cardiac MR imaging study. Radiology. 2009;250:363-370. https://doi.org/10.1148/radiol.2502080739.

Tables

Table 1 Patients' characteristics

Patient No.	Male	Age	BMI (kg/m^2)	Culprit vessel	Pain to balloon (hrs)	Peak cTnI (ng/ml)	Peak CK (U/L)	Peak CKMB (ng/ml)	WBCmax ($*10^9/L$)	Peak LDH (U/L)	LDL (mmol/L)	Peak BNP (pg/ml)	DM	HTN
1	Yes	82	33.78	LAD	8	110	2319	291.0	18.70	469	4.45	329	No	No
2	Yes	55	23.51	RCA	2	59	991	72.2	9.17	312	5.02	134	No	No
3	Yes	54	25.66	LAD	3	177	2475	174.0	8.26	459	3.64	72	No	Yes
4	Yes	52	24.68	RCA	8	>500	6418	177.4	12.13	1126	2.57	444	Yes	No
5	No	63	23.53	LAD	3	227	1583	116.3	12.69	444	4.89	88	No	Yes
6	Yes	75	25.01	LAD	5	>500	3554	395.0	11.29	584	3.35	495	No	No
7	No	59	23.73	LAD	12	>500	3554	395.0	11.29	584	3.35	495	No	Yes
8	Yes	54	29.65	LAD	4	349	5983	134.5	14.39	1143	3.61	99	Yes	No
9	Yes	72	29.05	LAD	12	>500	4763	337	14.73	845	2.57	380	Yes	Yes
10	Yes	46	31.14	RCA	10	19	222	29.7	12.24	252	3.45	121	No	Yes
11	Yes	64	22.31	LAD	12	373	4167	338	16.22	1299	2.65	720	No	No
12	No	53	30.92	LAD	3	53	1636	160	13.87	510	4.25	214	No	No
13	Yes	69	26.83	LM	2	171	1486	104	11.17	1289	4.95	794	No	No
14	Yes	74	22.68	LAD	6	45	964	84	9.58	383	3.39	732	Yes	Yes
Total	11 (79%)	62 ± 11	26.61 ± 3.66	NA	6 (3-11)	NA	2865.3 ± 1925.73	200.58 ± 125.34	12.55 ± 2.84	547 (429, 1130)	3.72 ± 0.86	365.50 ± 256.51	4 (29%)	6 (43%)

BMI, body mass index; *LAD*, left anterior descending coronary artery; *RCA*, right coronary artery; *cTnI*, cardiac troponin I; *CK*, creatine kinase; *CKMB*, creatine kinase-MB; *WBCmax*, maximum white blood cell; *LDH*, lactate dehydrogenase; *LDL*, low density lipoprotein; *BNP*, B-type natriuretic peptide; *DM*, diabetes mellitus; *HTN*, hypertension; *MI*, myocardial infarction; *PET*, positron emission tomography; *CMR*, cardiac magnetic resonance

Table 2 Correlation analysis between FAPI and serum biomarkers (n = 14)

Serum biomarkers	FAPI%			TBRmax			FAPI%×TBRmax		
	r	95%CI	P value	r	95%CI	P value	r	95%CI	P value
Peak CK, U/L	0.36	-0.11-0.86	0.20	0.20	-0.25-0.63	0.50	0.43	-0.12-0.81	0.12
Peak CKMB, ng/ml	0.79	0.60-0.94	**0.001**	0.03	-0.50-0.68	0.91	0.56	-0.05-0.91	**0.04**
WBCmax, $*10^9/L$	0.65	0.10-0.85	**0.01**	0.59	0.05-0.91	**0.03**	0.55	-0.06-0.88	**0.04**
Peak LDH, U/L	0.62	0.06-0.91	**0.02**	-0.25	-0.73-0.32	0.38	0.56	-0.01-0.91	**0.04**
LDL, mmol/L	-0.31	-0.72-0.22	0.29	-0.23	-0.67-0.31	0.43	-0.44	-0.80-0.13	0.12
Peak BNP, pg/ml	0.53	0.13-0.84	0.05	0.44	0.02-0.81	0.12	0.59	0.17-0.84	**0.03**

FAPI, fibroblast activation protein inhibitor; *TBRmax*, maximum target-to-background ratio; *CK*, creatine kinase; *CKMB*, creatine kinase-MB; *WBCmax*, maximum white blood cell; *LDH*, lactate dehydrogenase; *LDL*, low density lipoprotein; *BNP*, B-type natriuretic peptide; Bold P values, statistically significant (P<0.05)

Table 3 Correlation analysis between FAPI and baseline CMR parameters at patient level (n = 14)

CMR parameters	FAPI%			TBRmax			FAPI%×TBRmax		
	r	95%CI	P value	r	95%CI	P value	r	95%CI	P value
T2WI, %	0.83	0.54-0.95	**<0.001**	0.58	0.21-0.83	**0.03**	0.83	0.48-0.97	**<0.001**
LGE, %	0.72	0.32-0.94	**0.004**	0.54	0.11-0.81	**0.048**	0.81	0.46-0.96	**<0.001**
ECV, %	0.78	0.16-0.95	**0.002**	0.50	-0.15-0.85	0.09	0.72	0.19-0.92	**0.006**
LVEF, %	-0.72	-0.90- -0.24	**0.005**	-0.62	-0.86- -0.21	**0.02**	-0.73	-0.92- -0.33	**0.003**
EDV/BSA, ml/m^2	0.34	-0.27-0.75	0.23	0.11	-0.57-0.70	0.71	0.15	-0.40-0.66	0.62
ESV/BSA, ml/m^2	0.44	-0.14-0.80	0.12	0.42	-0.10-0.78	0.14	0.50	-0.02-0.80	0.07

CMR, cardiac magnetic resonance; *FAPI*, fibroblast activation protein inhibitor; *TBRmax*, maximum target-to-background ratio; *T2WI*, T2-weighted imaging; *LGE*, late gadolinium enhancement; *ECV*, extracellular volume; *LVEF*, left ventricular ejection fraction; *EDV*, end diastolic volume; *ESV*, end systolic volume; *BSA*, body surface area; Bold P values, statistically significant (P<0.05)

Table 4 Correlation analysis between baseline FAPI/CMR parameters and follow-up LV function (n = 9)

CMR parameters	LVEF, %		
	r	95%CI	P value
FAPI%	-0.24	-0.94-0.37	0.53
TBRmax	-0.73	-0.95- -0.33	**0.02**
FAPI%×TBRmax	-0.60	-0.95- 0.07	0.09
T2WI, %	-0.70	-0.94- -0.34	**0.03**
LGE, %	-0.45	-0.93-0.68	0.23
ECV, %	-0.74	-0.98- 0.06	**0.02**

CMR, cardiac magnetic resonance; *LVEF*, left ventricular ejection fraction; *FAPI*, fibroblast activation protein inhibitor; *TBRmax*, maximum target-to-background ratio; *T2WI*, T2-weighted imaging; *LGE*, late gadolinium enhancement; *ECV*, extracellular volume; Bold P values, statistically significant (P<0.05)

Figures

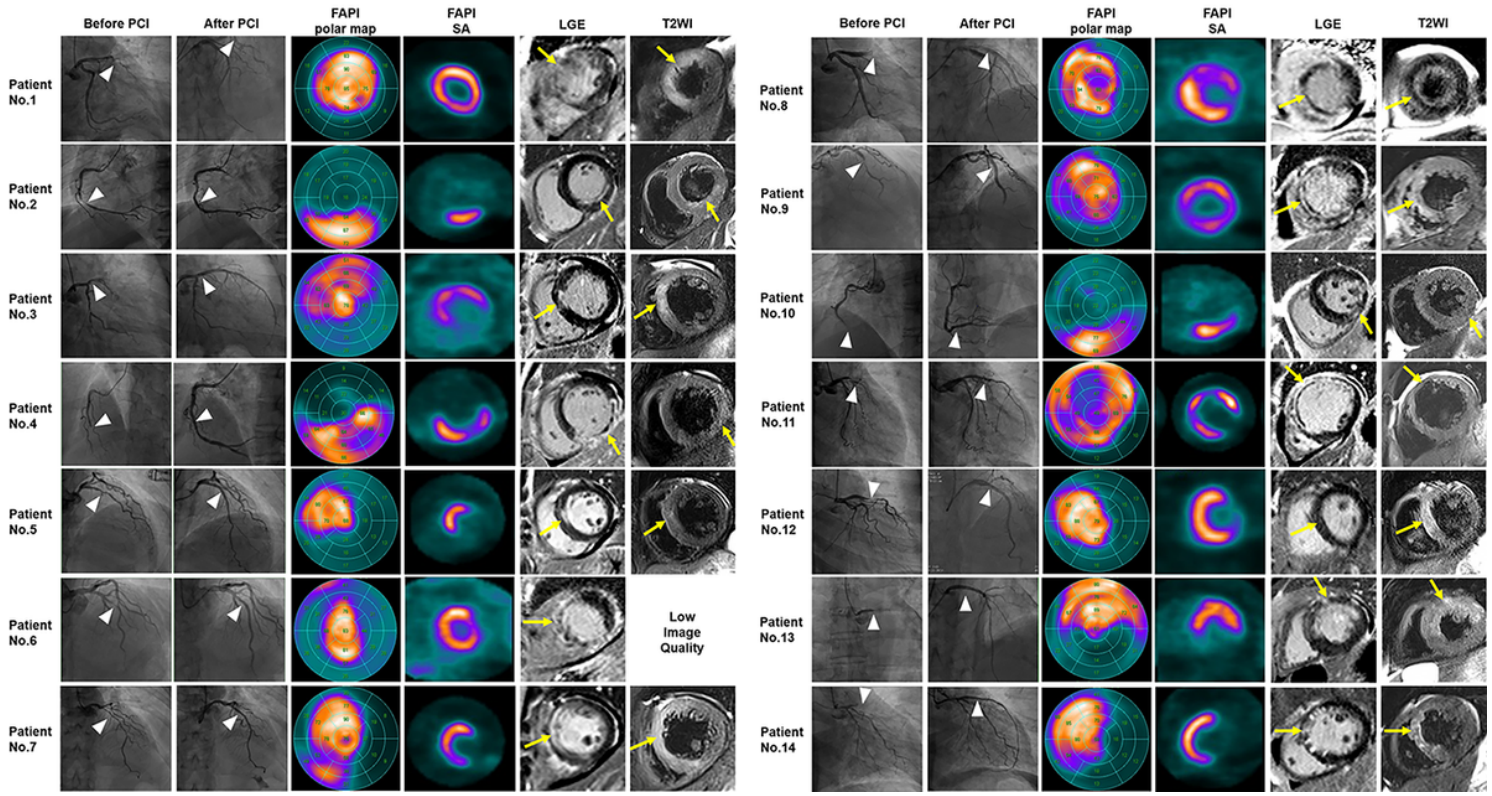

Figure 1

Detailed images of the 14 patients. Coronary angiographic images before (first column) and after PCI (second column) with the treated culprit vessel (white arrows). Polar maps (third column) and the selected short-axis images of FAPI (fourth column), LGE (fifth column), and T2WI (sixth column). FAPI uptake was observed in the culprit territory which was larger than the corresponding edematous and infarcted area (yellow arrows). PCI, percutaneous coronary intervention; FAPI, fibroblast activation protein inhibitor; SA, short-axis; LGE, late gadolinium enhancement; T2WI, T2-weighted imaging.

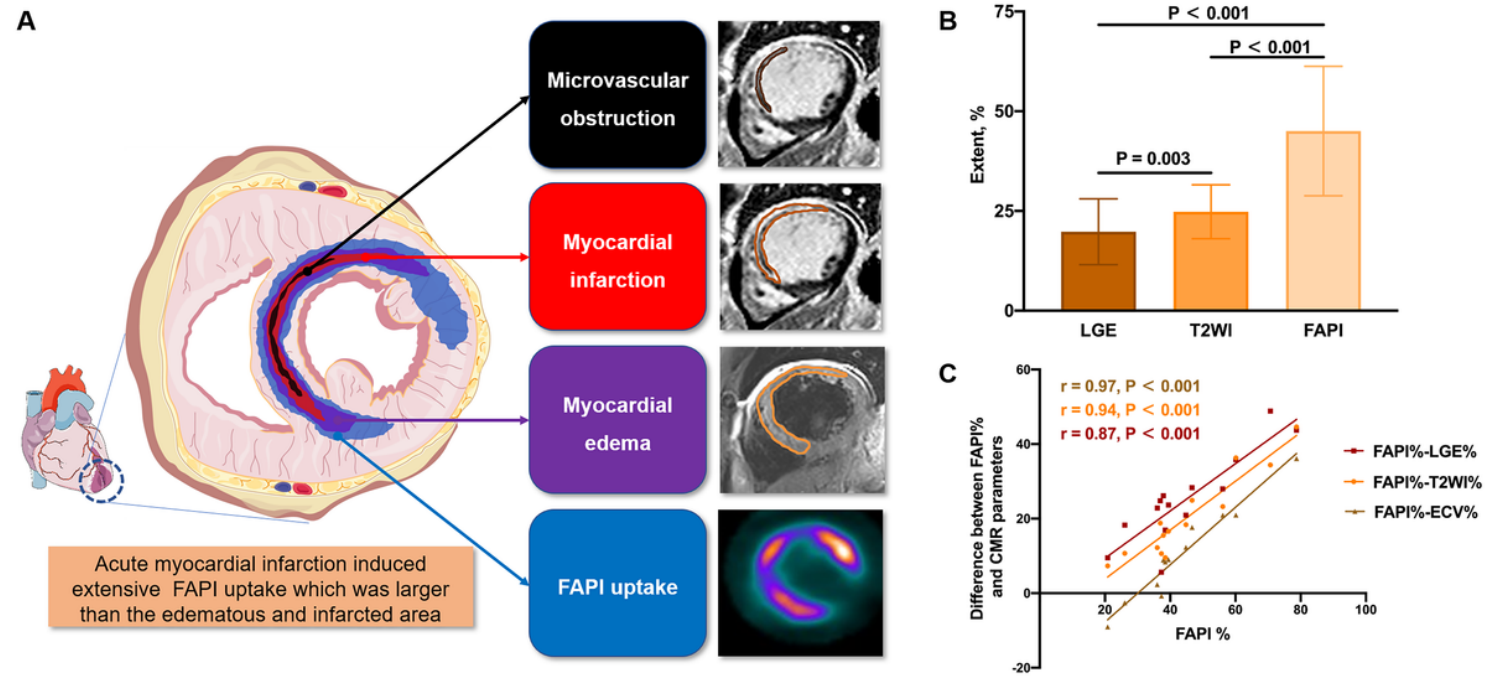

Figure 2

Comparison of FAPI uptake extent (FAPI%) and CMR parameters. A. A representative case and post-myocardial infarction illustration indicated FAPI uptake extent exceed that of CMR parameters. B. FAPI uptake extent was larger than the edematous and infarcted area. C. The differences between FAPI% and LGE%, T2WI%, ECV% increased with the FAPI uptake extent. FAPI, fibroblast activation protein inhibitor; CMR, cardiac magnetic resonance; LGE, late gadolinium enhancement; T2WI, T2-weighted imaging; ECV, extracellular volume.

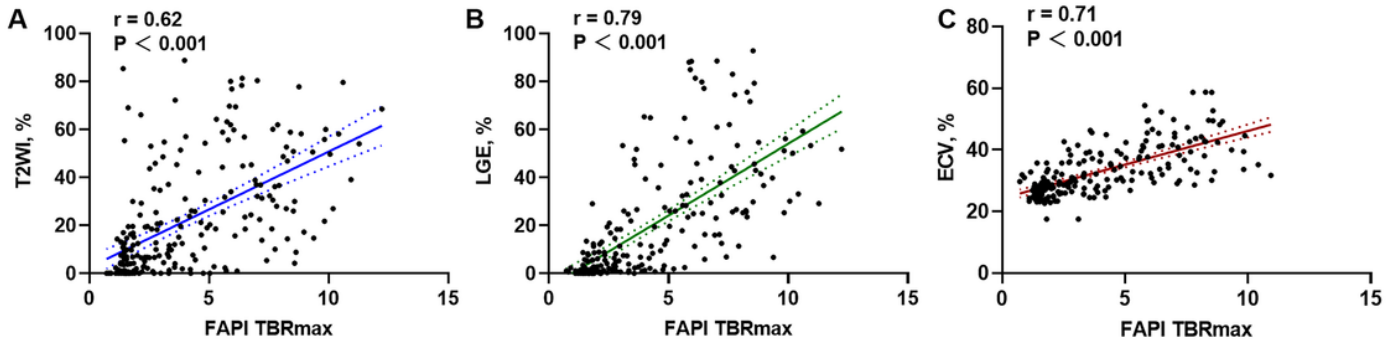

Figure 3

Spearman correlation analysis between FAPI and baseline T2WI% (A), LGE% (B), and ECV% (C) at segment level. FAPI, fibroblast activation protein inhibitor; CMR, cardiac magnetic resonance; TBRmax, maximum target-to-background ratio; T2WI, T2-weighted imaging; LGE, late gadolinium enhancement; ECV, extracellular volume.

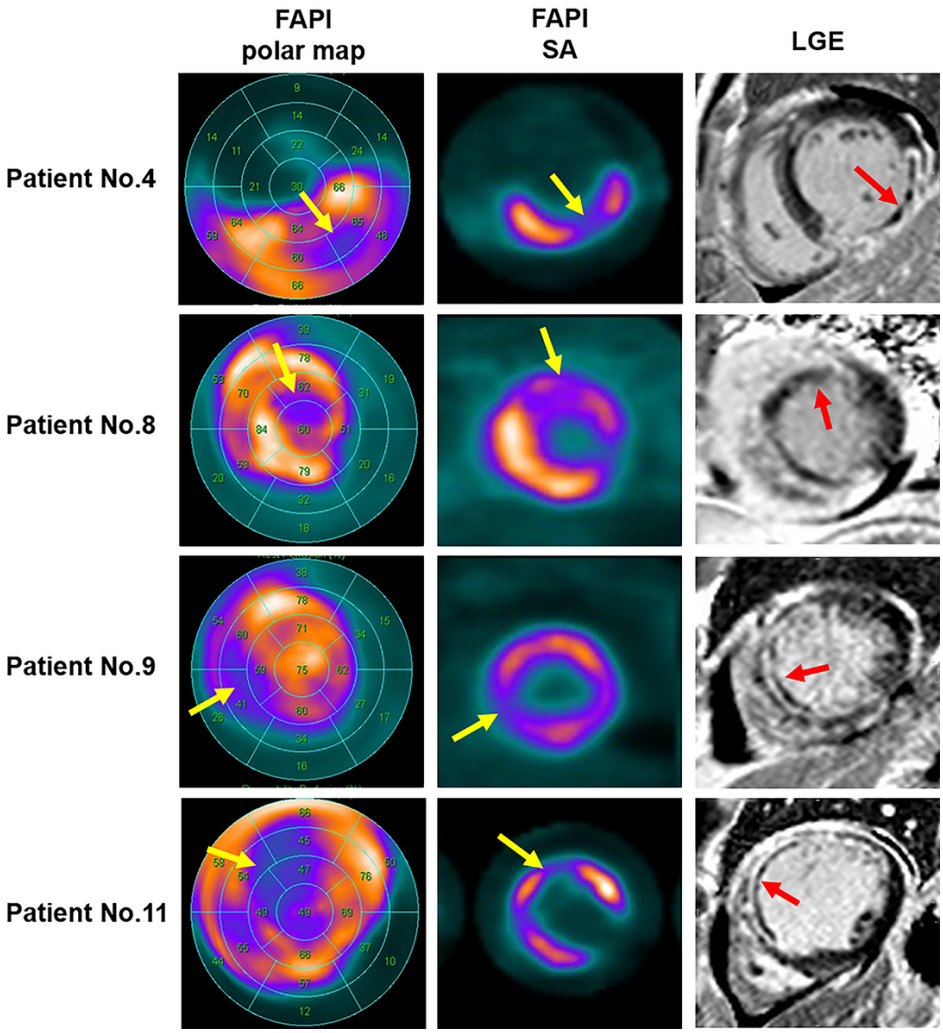

Figure 4

FAPI and LGE images in patients with MVO (No. 4, 8, 9, 11). MVO identified by LGE (red arrows) could be visualized as the hypo-uptake region within the hyper-uptake area by FAPI imaging (yellow arrows). FAPI, fibroblast activation protein inhibitor; SA, short-axis; LGE, late gadolinium enhancement; MVO, microvascular obstruction.

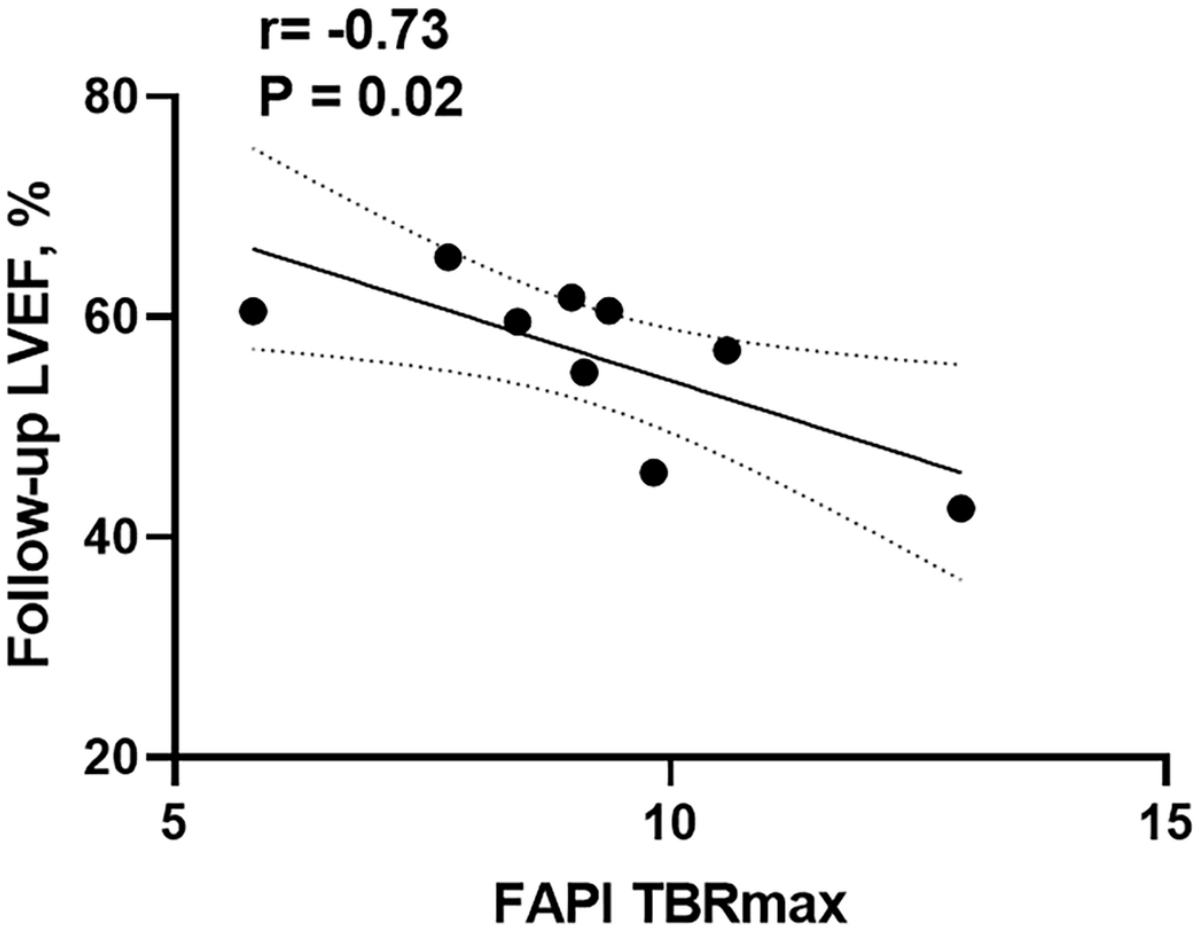

Figure 5

Relationship between baseline FAPI intensity and convalescent LVEF. Myocardial FAPI uptake intensity was inversely related with convalescent LVEF. FAPI, fibroblast activation protein inhibitor; TBRmax, maximum target-to-background ratio; LVEF, left ventricular ejection fraction.